Journal of Power Sources 232 (2013) 7–11

Contents lists available at SciVerse ScienceDirect

Journal of Power Sources

journal homepage: www.elsevier.com/locate/jpowsour

Short communication

Preparation of a spinel $LiMn_2O_4$ single crystal film from a MnO wafer

Mitsunori Kitta*, Tomoki Akita, Masanori Kohyama

Research Institute for Ubiquitous Energy Devices, National Institute of Advanced Industrial Science and Technology (AIST), 1-8-31 Midorigaoka, Ikeda, Osaka 563-8577, Japan

HIGHLIGHTS

- Single crystalline spinel $LiMn_2O_4$ film was prepared from MnO wafer.
- $LiMn_2O_4$(100), (110) and (111) films were formed on MnO(100), (110) and (111) wafers.
- Atomically flat terraces with steps of a minimum height of about 0.5 nm were confirmed on the (111) film surface.
- Prepared (111) film showed two-steps charge–discharge voltage profile that is typical electrochemical behavior of $LiMn_2O_4$.

ARTICLE INFO

Article history:
Received 3 September 2012
Received in revised form
19 December 2012
Accepted 24 December 2012
Available online 11 January 2013

Keywords:
Li-ion battery
Positive electrode materials
$LiMn_2O_4$
Thin-film preparation
Electrochemical and surface study

ABSTRACT

Spinel $LiMn_2O_4$ is a very promising material for positive electrodes in a wide range of Li-ion battery applications due to its lower cost and more environmental friendliness than any other electrode materials. Although the bulk properties of $LiMn_2O_4$ have been studied intensively, there have been few reports about the structure and properties of $LiMn_2O_4$ surfaces in spite of the importance of solid/electrolyte interfaces. This is caused by the difficulty in preparing $LiMn_2O_4$ samples with accessible flat surfaces suitable for atomistic observations. To address this, we have successfully prepared a single crystalline $LiMn_2O_4$ film with an atomically flat surface by solid-state reaction from a MnO wafer with $LiOH.H_2O$ powder. X-ray diffraction (XRD) reveals the single crystalline growth of $LiMn_2O_4$ films depending on the orientation of a MnO wafer. Atomic force microscopy observations revealed that a $LiMn_2O_4$ (111) film has an atomically flat surface with steps of a {111} interlayer height. Electron energy-loss spectroscopy (EELS) study of the (111) film revealed that the sample consists of Li, Mn^{3+} and Mn^{4+} with a composition similar to $LiMn_2O_4$. The (111) film sample is also investigated by cyclic voltammetry and galvanostatic experiments, revealing that a crushed powder sample from the film has electrochemical activity as usual positive electrode material.

1. Introduction

Lithium manganese spinel, $LiMn_2O_4$, is one of the most prominent cathode materials for rechargeable lithium batteries due to its low cost and environmental friendliness [1,2]. $LiMn_2O_4$ has cubic spinel structure (space group: Fd-3m), where oxygen ions form a cubic-close-packed lattice, and Li and Mn ions are located at tetrahedral (8a) and octahedral (16d) sites, respectively. Electrochemical extraction of Li ions from the tetrahedral site occurs at 4 V, associated with the phase change of $LiMn_2O_4$ with the average Mn valence of +3.5 to λ-MnO_2 with Mn^{4+}.

Many studies of $LiMn_2O_4$ deal with its electrochemical characteristics in lithium cells [1–3] as well as its structural and physical properties [4–7] by X-ray diffraction, [8,9] neutron diffraction, [7,10] nuclear magnetic resonance, [8,11,12] XAFS [6,13,14], magnetism [5,15] and Raman spectroscopy [16]. Studies on the bulk properties have been contributed to a better understanding of the reaction mechanism in the bulk electrode. However, it is also important to investigate the electrochemical reaction at the electrode surface, so as to improve the power and calendar-life characteristics of $LiMn_2O_4$ [17,18]. Thus, a lot of studies focusing on the surface properties have been performed by using spectroscopy or microscopy techniques such as surface X-ray diffraction [19,20], X-ray photoelectron spectroscopy [21,22], IR spectroscopy [23,24], and scanning probe microscopy (SPM) [25–28]. Especially, the SPM observation allows us to obtain the direct image of the electrode-surface structure at nano- or atomic scales, and so it should provide deep insights into the electrochemical surface reaction, which cannot be obtained by usual spectroscopic investigations.

To perform the SPM observation, sample surfaces should be as flat as possible to obtain images with high resolution. However, it is difficult to prepare $LiMn_2O_4$ films with atomically flat surfaces by

* Corresponding author. Tel.: +81 072 751 8703; fax: +81 072 751 9714.
E-mail address: m-kitta@aist.go.jp (M. Kitta).

0378-7753/$ – see front matter © 2013 Elsevier B.V. All rights reserved.
http://dx.doi.org/10.1016/j.jpowsour.2012.12.096

epitaxial methods or by any other thin-film preparation methods, because the crystallinity or morphology of a film seriously depends on various conditions such as substrates, temperature and atmosphere. It is highly desirable to prepare a well-characterized $LiMn_2O_4$ single crystalline film with atomically flat surfaces, but such single crystalline films with good quality have not yet been synthesized.

In our preceding study, we developed the method to prepare a $Li_4Ti_5O_{12}$ film on a TiO_2 wafer surface by using conventional solid-state reaction [29]. This preparation method enables us to obtain a single crystalline film with high quality and well-defined atomically flat surfaces suitable for SPM observation. In the present study, we apply this scheme to obtain a single crystalline $LiMn_2O_4$ film on a MnO wafer.

2. Materials and methods

A $LiMn_2O_4$ crystal is formed on a MnO wafer by conventional solid-state reaction. Because both the $LiMn_2O_4$ and MnO (space group: Fm-3m, a = 4.45 Å) crystals belong to the cubic system, it is considered that the growth orientation of a $LiMn_2O_4$ crystalline film can be controlled by selecting the surface orientation of a MnO wafer. Thus we used (100), (110) and (111) wafers of MnO single crystals (purchased from Crystal Base Co., Ltd) of $2 \times 2 \times 0.5$ mm^3 with one side polished. Each wafer was cleaned in acetone by ultrasonic cleaner, and was calcined at 1173 K for 15 h in air using an alumina crucible with $LiOH.H_2O$ powder (Wako, LTD) to produce $LiMn_2O_4$. After calcinations, a film of about 150 μm thickness was formed on a MnO wafer.

X-ray diffraction data were recorded by intelligent X-ray diffractometer (SmartLab, Rigaku) with Cu Ka1 radiation. The beam diameter was about 10 mm^2. The orientation of the synthesized film was characterized by out-of-plane and pole-figure measurement techniques. The surface morphology and flatness of the film were investigated by atomic force microscopy (AFM) (NanoNavi-II, SII) with DFM mode. The elemental analysis of the film was performed by transmission electron microscopy (TEM) (JEM-3000F, JEOL) equipped with electron energy-loss spectroscopy (EELS) using Gatan imaging filter (GIF, GATAN Inc.) at 97 keV.

The electrochemical property of the synthesized film was evaluated by cyclic voltammetry and galvanostatic charge–discharge experiments. A test-type electrochemical cell (HS-cell, Hohsen Corp.) was used for both experiments. The counter electrode was constructed by a lithium foil and the electrolyte was a 1:1 mixture of ethylene carbonate (EC) and dimethyl carbonate (DMC) containing 1 M $LiPF_6$. The synthesized (111) film was flaked from a wafer and crushed for a cathode active material. The electrode consists of 80 wt% active material, 10 wt% ketzen black, and 10 wt% Teflon binder. These components were dispersed in ethyl alcohol and sheeted by pressing and drying in dry air for 12 h. After the cells were assembled in dry air, the charge–discharge cycle was galvanostatically carried out at a rate of 1/3.2 C with a cut-off voltage of 3.5–4.5 V (*vs* Li/Li$^+$) for five cycles. The cyclic voltammetry experiments were carried at a scan rate of 0.05 mV s^{-1} for three cycles in the room temperature.

3. Results and discussion

3.1. XRD measurements of synthesized films

Fig. 1 shows the optical micrographs of the synthesized films grown on MnO wafers with different orientations. We can see continuous facet edges on each surface, which have different features depending on the wafer orientation. The facet edges with angles of 90°and 60°are generated on the films grown on the MnO (100) and (111) wafers, respectively, and the parallel facet edges are observed on the film grown on the MnO (110) wafer. All these features indicate that a highly-oriented single crystal with a single domain is formed as a film in each system.

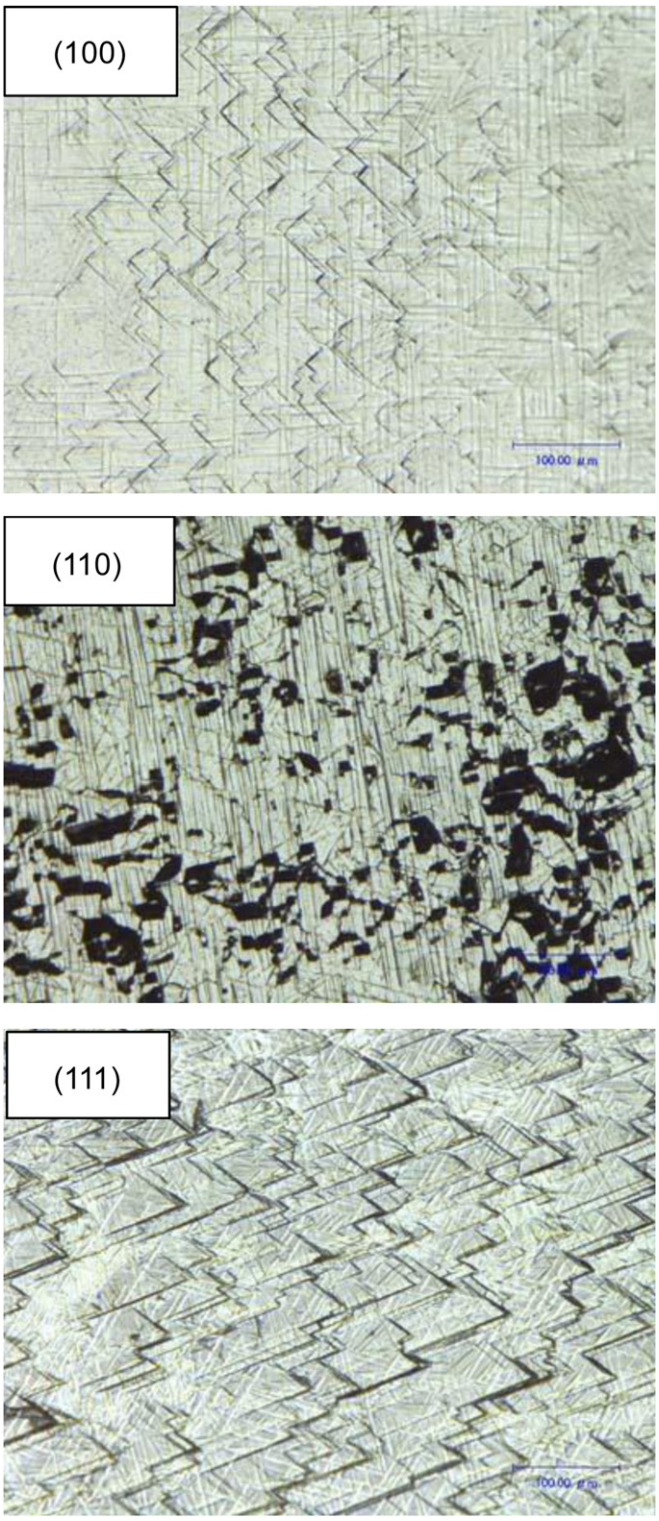

Fig. 1. Optical micrographs of prepared films formed on MnO (100) (110) and (111) wafers. The pictures were acquired by Digital Microscope at ×500.

Fig. 2(A) shows the out-of-plane XRD spectra of the synthesized films grown on the MnO (100), (110) and (111) wafers as lines (a),

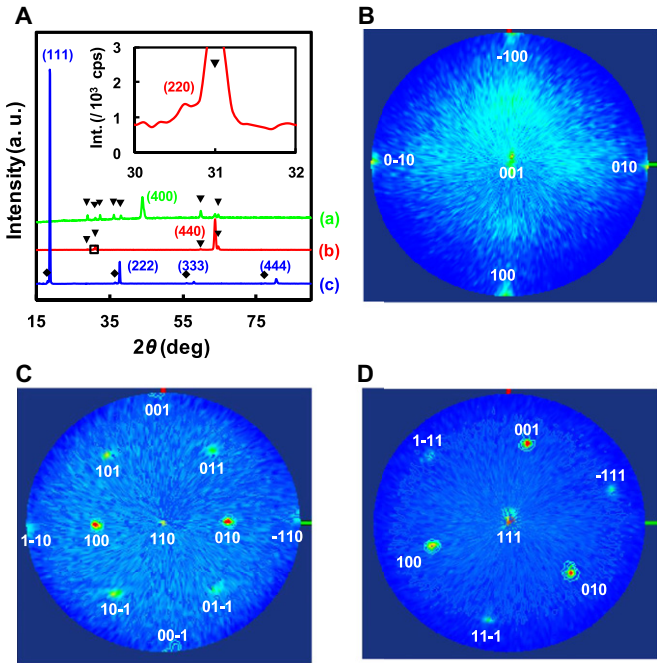

Fig. 2. Out-of-plane XRD spectra of the films formed on MnO wafers (A). Spectra (a), (b) and (c) indicate those of the films formed on the (100), (110) and (111) wafers, respectively. An inset shows the magnification near the (220) diffraction position in spectrum (b). Pole figures of the films formed on the MnO (100) (B), (110) (C) and (111) (D) wafers.

(b) and (c), respectively. The film formed on the MnO (100) wafer has the strongest diffraction line at about 43.9° of 2θ, corresponding to the (400) diffraction peak of a spinel crystal (a = 8.240 Å). Other small peaks marked by filled triangles ▼ in line (a) are assigned as those of Mn_3O_4 (Hausmannite, spaces group of $I4_1/amd$ ICDD PDF#073-6699) [30]. The film formed on the MnO (100) wafer is mainly a (100)-oriented $LiMn_2O_4$ spinel crystal, while it contains randomly-oriented Mn_3O_4 as an impurity phase.

In the diffraction spectrum of the film formed on the MnO (110) wafer (line (b) of Fig. 2(A)), the strongest peak at about 63.8°is identified as the (440) line of a spinel crystal (a = 8.245 Å), while the other small peaks with filled triangles ▼ are assigned as those of Mn_3O_4, similarly to the (100) film. As shown in the inset in Fig. 2(A), there is a diffraction peak at about 30.6° of 2θ, corresponding to the (220) diffraction line of a spinel crystal (a = 8.245 Å). It can be said that the film formed on the MnO (110) wafer is mainly a (110)-oriented $LiMn_2O_4$ spinel crystal, while it contains a Mn_3O_4 phase, similarly to the (100) film.

In the diffraction spectrum of the film formed on the MnO (111) wafer (line (c) of Fig. 2(A)), the strongest diffraction line at about 18.5° of 2θ is identified as the (111) diffraction peak of a spinel crystal (a = 8.255 Å), and we can see the (222), (333), and (444) diffraction lines as the epitaxial (111) film [19]. All these peaks indicate that the formed film is basically a (111)-oriented $LiMn_2O_4$ single crystal. There is a weak diffraction peak marked by a filled square ◆ at about 17.9° of 2θ, which is a little smaller than the angle of the strongest (111) line. Similar weak peaks marked by filled squares are also observed in a little lower side of the angles of the (222), (333) and (444) diffraction lines. All these weak peaks can be assigned as the diffraction of a different spinel crystal (a = 8.52 Å), $Li_{1.223}Mn_{2.447}O_4$ (ICDD PDF#054-0261, a = 8.48 Å) [31], formed with the same orientation as the $LiMn_2O_4$ crystal.

This impurity phase is also expressed as $LiMn_2O_{3.27}$, which means the deficiency of 0.73 O from the chemical composition of $LiMn_2O_4$. The formation of $LiMn_2O_{3.27}$ should be caused by the deficiency in oxygen supply during the growth of $LiMn_2O_4$ from the MnO wafer. The ratio of O/Mn has to become twice as much during the formation of $LiMn_2O_4$ from MnO, and thus enough oxygen has to be supplied. However, it is possible that the oxygen supply is not enough inside the film during the growth process in air, leading to the formation of the oxygen deficient phase as $LiMn_2O_{3.27}$. Thus this phase should exist rather deep inside the film, while detailed examination is not so easy at present. The abundance ratio of this phase is about 1.6%, evaluated from the peak intensity ratio. Thus the (111) film can be regarded to be almost a single phase.

Here, the spinel $LiMn_2O_4$ single crystal has the lattice constant of 8.248 Å [32], and the spinel crystal films formed on the MnO (100), (110) and (111) wafers have similar values of the lattice constant. Thus we conclude that $LiMn_2O_4$ (100), (110) and (111) films are indeed formed on the MnO (100), (110) and (111) wafers, respectively. Fig. 2(B)–(D) shows the pole figures of the (100), (110) and (111) films. Clear diffraction spots are observed in all the figures, indicating that each film consists of a single domain crystal. Note that the spot size of X-ray is the millimeter scale. It can be said that highly-oriented $LiMn_2O_4$ single crystalline films can be prepared using a MnO wafer, and that the orientation of film growth can be controlled by selecting the orientation of a MnO wafer.

The impurity phases as Mn_3O_4 or $Li_{1.223}Mn_{2.447}O_4$ may exist as different domains in each film, while the $LiMn_2O_4$ spinel crystal in each film should be a single crystal in a single domain due to the XRD measurement and surface-facet observation. Both the Mn_3O_4 and $Li_{1.223}Mn_{2.447}O_4$ phases should be formed rather deep inside the film, not near the surface. Mn_3O_4 is considered to be generated near the MnO substrate due to the deficiency of Li supply, as $Li_{1.223}Mn_{2.447}O_4$ is generated due to the deficiency of oxygen. In the present study, aiming to obtain atomically flat $LiMn_2O_4$ surfaces, these impurity phases do not seem to induce serious problems on the surfaces, due to their places and small contents in each film.

3.2. Atomic force microscopy

We examined the surface structure and roughness of the formed (100), (111) and (111) $LiMn_2O_4$ films by AFM as shown in Fig. 3. The structure and morphology of the surfaces are greatly dependent on the film orientation. The (100) film surface shown in Fig. 3(A) has complex morphology. This does not mean that the (100) film is a polycrystalline or microcrystalline, but the crystal surface of the (100) film itself is rough. The roughness was evaluated as 0.3 nm of *Ra* value. This value itself is not so large, and we can say that this surface is almost atomically flat.

The (110) film surface shown in Fig. 3(B) does not have clear structure, while lines running diagonally may reflect the crystal character of the $LiMn_2O_4$ (110) surface. However, the roughness along the direction crossing the lines is nanometer scale, and it is not so homogeneous. This may be caused by the fact that the surface of a (110) film is not so stable as that of a (100) film [33].

On the other hand, clear steps and terraces can be seen with high regularity on the surface of the (111) film shown in Fig. 3(C). Fig. 3(D) shows the surface profile along the line in Fig. 3(C). A number of terraces have around 100 nm width with roughness less than 0.1 nm, and no other characteristic constructions are observed on the terraces, suggesting that we could prepare the atomically flat surface. On the line profile, steps of about 0.5 nm height are observed. The minimum step height is confirmed as about 0.5 nm in any places, and almost all higher steps have the heights of integer multiples of 0.5 nm. Thus the single step height should be about 0.5 nm on this surface, corresponding to the {111} interplanar spacing (0.477 nm) of the spinel $LiMn_2O_4$ structure.

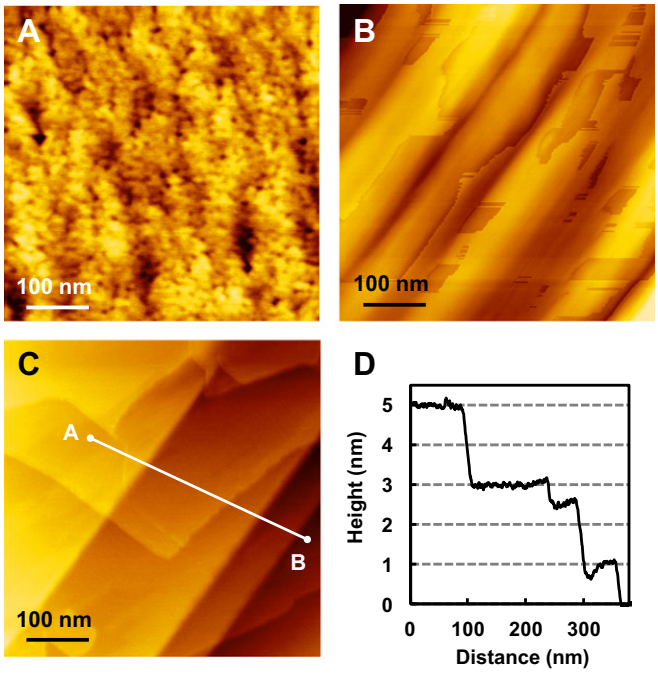

Fig. 3. AFM images of the surfaces of the (100) (A), (110) (B) and (111) (C) films. All the data was acquired at scan area of 500 nm × 500 nm. The surface line profile is shown in (D) for the line A-B in (C).

From the AFM results, we can conclude that the $LiMn_2O_4$ (111) film has a well-defined atomically flat surface. The (111) film has the best quality among the examined films. As explained above, the (111) film has no impurity Mn_3O_4 phase, except for a small content of $Li_{1.223}Mn_{2.447}O_4$. All these points can be understood by the fact that the (111) surface is the most stable in a $LiMn_2O_4$ crystal [33]. In other words, a $LiMn_2O_4$ (111) film is easy to grow, compared to $LiMn_2O_4$ (100) and (110) films.

3.3. Electron energy-loss spectroscopy study of prepared (111) film

Fig. 4 shows EEL spectra of the prepared (111) film. The film was scratched from a MnO wafer and crashed to prepare the thin specimen. EEL spectra were acquired from Li-*K* edge and Mn-*L* edge regions to investigate the chemical components and chemical states of Mn ions in the prepared film.

In the Li-*K* edge energy region spectra shown in Fig. 4(A), there exists an energy-loss peak at 60.7 eV in the (111) sample, which is also observed in the standard $LiMn_2O_4$ powder (purchased from Nikki Chemicals, Co.) and Li_2MnO_3 powder. However, the Mn_2O_3 sample has no peak in this energy position. Thus we can say that this peak is not caused by Mn but caused by Li. The intensity of this peak in the prepared film is similar to the corresponding peak in $LiMn_2O_4$, while it is weaker than the corresponding peak in Li_2MnO_3. This suggests that the Li/Mn component ratio in the prepared (111) film is similar to that in $LiMn_2O_4$, and is lower than that in Li_2MnO_3.

The chemical state of Mn in the (111) film can be examined by the Mn-*L* edge spectrum shown in Fig. 4(B). Here, it is known that the shape of Mn-L_3 edge spectrum is varied according to the valence state of Mn. This feature can be actually observed in the L_3 edge spectra of Li_2MnO_3 (Mn^{4+}) and Mn_2O_3 (Mn^{3+}). The spectrum of Li_2MnO_3 containing only Mn^{4+} has two main peaks assigned as No. 1 and No. 3, and the spectrum of Mn_2O_3 (Mn^{3+}) has only one peak assigned as No. 2. These features are the same as the other

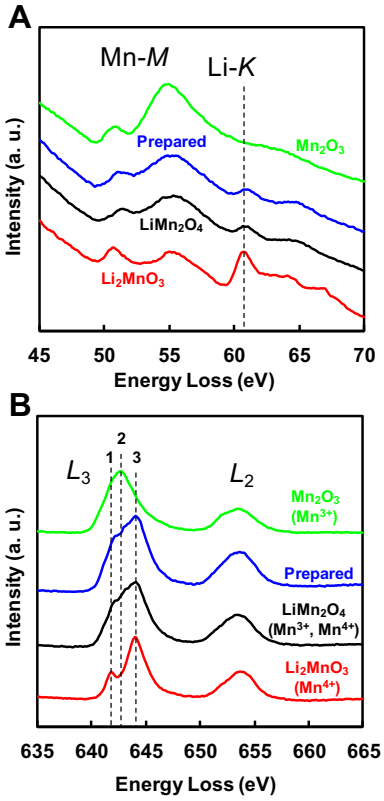

Fig. 4. (A) EEL spectra of various Li–Mn–O samples in the Li-*K* edge region. All the spectra were normalized by the Mn-*M* edge peak intensity. (B) EEL spectra in the Mn-*L* edge region. All the spectra were normalized by the L_3 edge peak intensity.

minerals containing Mn [34]. On the other hand, $LiMn_2O_4$ containing both Mn^{3+} and Mn^{4+} has one main peak at No. 3 concerning Mn^{4+} and two shoulder peaks at No. 1 and No. 2, concerning Mn^{4+} and Mn^{3+}, respectively, as observed by the X-ray absorption study [14]. This feature is also observed in the prepared (111) film. From all the results of Li-*K* edge and Mn-*L* edge spectra, we can conclude that the prepared film is $LiMn_2O_4$.

3.4. Electrochemical experiments

Electrochemical properties of the prepared film were investigated by cyclic voltammetry. Fig. 5(A) shows three cycles of cyclic voltammogram for the electrode, made of crushed powder of the $LiMn_2O_4$ (111) film, with a scan rate of 0.05 mV s^{-1} for 3.5V–4.5 V potential region. Two pairs of separated oxidation peaks at 4.05 and 4.21 V, and reduction peaks at 3.91 and 4.06 V, obviously reflect the two-step reversible intercalation and deintercalation of lithium between $LiMn_2O_4$ and λ-MnO_2. The ratio of the anodic peak height to the cathodic peak height (I_{pa}/I_{pc}) is nearly 1 (0.91) and the areas of the two redox peaks are almost equal. These results indicate that the intercalation and deintercalation of Li ions occur reversibly and that each reaction occurs as the two-stage process. Furthermore, the CV curves of the three cycles are all similar, indicating good reversibility.

Fig. 5(B) shows the charge–discharge characteristics in the first five cycles at a constant performance rate of 1/3.2 C between 4.5 and 3.5 V. There are two distinct potential plateaus at about 4.02 and 4.15 V in the charge curves, and at about 4.10 and 3.95 V in the discharge curves, respectively. These potential plateaus correspond to the redox current peaks in the voltammetry curves in Fig. 5(A), and are characteristic of the $LiMn_2O_4$ spinel structure [2]. The

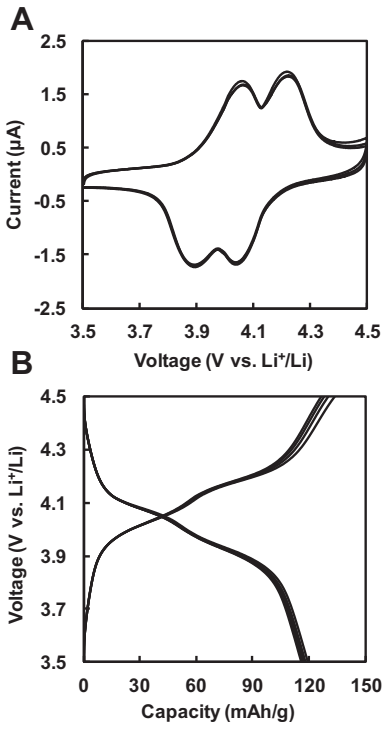

Fig. 5. (A) Three cycles of cyclic-voltamograms of an electrochemical cell with a cathode made of crushed powder of the synthesized (111) film. (B) Five cycles of galvanostatic charge–discharge property of the synthesized (111) film.

discharge capacity in the first cycle was estimated as 116 mAh g^{-1}, which is identical to the result of conventional $LiMn_2O_4$ spinel. The capacity at the fifth cycle is 113 mAh g^{-1}, which is about 97% of the first cycle, indicating the stable charge–discharge cycle property of the prepared film.

In the present study, crushed powder samples made of the prepared film were used in the electrochemical experiments. Of course, it is desirable to examine the electrochemical properties of the prepared film directly as a film sample. At present, it is not possible to perform such experiments, because of the low electron conductivity of the prepared $LiMn_2O_4$ film. We have tried to obtain the galvanostatic charge–discharge curves for the prepared (111) film, while the current density was decreased till the instrumental limit due to the low conductivity. Even in such an experiment, the voltage flat was observed in both the charge and discharge curves, indicating the electrochemical activity of the prepared film. However, we could not obtain the characteristic *two-stage* voltage profile in such a low current density. Here we would like to emphasize that we successfully generate highly-oriented single crystal $LiMn_2O_4$ (111) films with atomically flat surfaces and with usual electrochemical activity in powder forms. The present technique should open the way to investigate both the surface electrochemical reaction and surface structural change in $LiMn_2O_4$ as recent studies of $Li_4Ti_5O_{12}$ [35].

4. Conclusion

We had successfully prepared spinel $LiMn_2O_4$ single crystalline films on MnO wafers by conventional solid-state reaction. We produced films of about 150 μm thickness on the MnO (100), (110) and (111) surfaces. Out-of-plane and pole-figure XRD techniques revealed that the formed films are highly-oriented (100), (110) and (111) spinel single crystals. The AFM observation revealed that the (111) film is well crystallized and has an atomically flat surface with steps of a minimum height of 0.5 nm, corresponding to the {111} interplanar spacing in spinel $LiMn_2O_4$. The EELS analysis revealed that the prepared (111) film has the Li/Mn component ratio similar to that in a standard $LiMn_2O_4$ crystal sample, and that the film contains both Mn^{3+} and Mn^{4+} similarly to $LiMn_2O_4$. In the electrochemical experiments, the crushed powder sample from the formed film is really active for reversible Li insertion/extraction at about 3.9 V and 4.1 V *vs* Li^+/Li as usual $LiMn_2O_4$. Our prepared films should be effective to atomic-level studies of electrochemical phenomena of $LiMn_2O_4$ surfaces by using *in-situ* or *ex-situ* SPM investigation and other spectroscopic or microscopic techniques.

Acknowledgement

The authors thank Mr. Hisashi Yashiro for X-ray diffraction analysis. This work was supported by the Japan Society for the Promotion of Science (JSPS Grant-in-Aid for Scientific Research (B) 22360276).

References

[1] M.M. Thackeray, P.J. Johnson, L.A. de Picciotto, Mater. Res. Bull. 19 (1984) 179–187.
[2] M.M. Thackeray, Prog. Solid State Chem. 25 (1997) 1–71.
[3] R.J. Gummow, A. de Kock, M.M. Thackeray, Solid State Ionics 69 (1994) 59–67.
[4] A. Yamada, M. Tanaka, Mater. Res. Bull. 30 (1995) 715–721.
[5] Y. Shimakawa, T. Numata, J. Tabuchi, J. Solid State Chem. 131 (1997) 138–143.
[6] H. Yamaguchi, A. Yamada, H. Uwe, Phys. Rev. B 58 (1998) 8–11.
[7] P. Strobel, F.L. Cras, L. Seguin, M. Anne, J.M. Tarascon, J. Solid State Chem. 135 (1998) 132–139.
[8] Y.J. Lee, F. Wang, S. Mukerjee, J. McBreen, C.P. Greya, J. Electrochem. Soc. 147 (2000) 803–812.
[9] X. Sun, X.Q. Yang, M. Balasubramanian, J. McBreen, Y. Xia, T. Sakai, J. Electrochem. Soc. 149 (2002) A842–A848.
[10] M. Yonemura, A. Yamada, H. Kobayashi, M. Tabuchi, T. Kamiyama, Y. Kawamoto, R. Kanno, J. Mater. Chem. 14 (2004) 1948–1958.
[11] Y.J. Lee, F. Wang, C.P. Grey, J. Am. Chem. Soc. 120 (1998) 12601–12613.
[12] C.P. Grey, N. Dupre, Chem. Rev. 104 (2004) 4493–4512.
[13] Y. Shiraishi, I. Nakai, T. Tsubata, T. Himeda, F. Nishikawa, J. Solid State Chem. 133 (1997) 587–590.
[14] R.S. Liu, L.Y. Jang, J.M. Chen, Y.C. Tsai, Y.D. Hwang, R.G. Liu, J. Solid State Chem. 128 (1997) 326–329.
[15] A.S. Wills, N.P. Raju, J.E. Greedan, Chem. Mater. 11 (1999) 1510–1518.
[16] W. Huang, R. Frech, J. Power Sources 81–82 (1999) 616–620.
[17] G. Amatuccib, A.D. Pasquierb, A. Blyra, T. Zhengb, J.M. Tarascona, Electrochim. A 45 (1999) 255–271.
[18] J. Cho, G.B. Kim, H.S. Lim, C.S. Kim, S.I. Yoo, Electrochem. Solid State Lett. 2 (1999) 607–609.
[19] M. Hirayama, N. Sonoyama, M. Ito, M. Minoura, D. Mori, A. Yamada, K. Tamura, J. Mizuki, R. Kanno, J. Electrochem. Soc. 154 (2007) A1065–A1072.
[20] M. Hirayama, H. Ido, K. Kim, W. Cho, K. Tamura, J. Mizuki, R. Kanno, J. Am. Chem. Soc. 132 (2010) 15268–15276.
[21] A. Schechter, D. Aurbach, H. Cohen, Langmuir 15 (1999) 3334–3342.
[22] K. Araki, N. Sato, J. Power Sources 124 (2003) 124–132.
[23] D. Aurbach, K. Gamolsky, B. Markovsky, G. Salitra, Y. Gofer, U. Heider, R. Oesten, M. Schmidt, J. Electrochem. Soc. 147 (2000) 1322–1331.
[24] D. Aurbach, M.D. Levi, E. Levi, H. Teller, B. Markovsky, J. Electrochem. Soc. 145 (1998) 3024–3034.
[25] T. Doi, M. Inaba, H. Tsuchiya, S.-K. Jeong, Y. Iriyama, T. Abe, Z. Ogumi, J. Power Sources 180 (2008) 539–545.
[26] Y. Matsuo, R. Kostecki, F. McLarnon, J. Electrochem. Soc. 148 (2001) A687–A692.
[27] M. Inaba, T. Doi, Y. Iriyama, T. Abe, Z. Ogumi, J. Power Sources 81-82 (1999) 554–557.
[28] K. Kuriyama, A. Onoue, Y. Yuasa, K. Kushida, Surf. Sci. 601 (2007) 2256–2259.
[29] M. Kitta, T. Akita, Y. Maeda, M. Kohyama, Appl. Surf. Sci. 258 (2012) 3147–3151.
[30] B. Chardon, F. Vigneron, J. Magn. Magn. Mater. 58 (1986) 128–134.
[31] V. Massarotti, D. Capsoni, M. Bini, Solid State Commun. 122 (2002) 317–322.
[32] J. Akimoto, Y. Takahashi, Y. Gotoh, S. Mizuta, Chem. Mater. 12 (2000) 3246–3248.
[33] M.-R. Huang, C.-W. Lin, H.-Y. Lu, Appl. Surf. Sci. 177 (2001) 103–113.
[34] L.A.J. Garvie, A.J. Craven, Phys. Chem. Miner. 21 (1994) 191–206.
[35] M. Kitta, T. Akita, Y. Maeda, M. Kohyama, Langmuir 28 (2012) 12384–12392.